**Article**
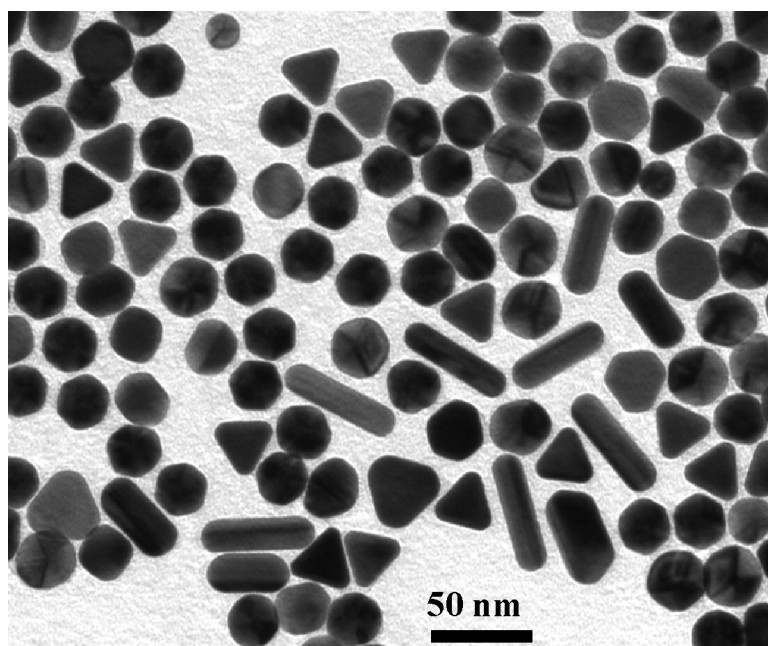
# Dependence of Crystal Growth of Gold Nanoparticles on the Capping Behavior of Surfactant at Ambient Conditions

Mandeep Singh Bakshi, Shweta Sachar, Gurpreet Kaur, Poonam Bhandari,
Gurinder Kaur, Mark C. Biesinger, Fred Possmayer, and Nils O. Petersen

## More About This Article

Additional resources and features associated with this article are available within the HTML version:

- Supporting Information
- Links to the 1 articles that cite this article, as of the time of this article download
- Access to high resolution figures
- Links to articles and content related to this article
- Copyright permission to reproduce figures and/or text from this article

**View the Full Text HTML**

# Dependence of Crystal Growth of Gold Nanoparticles on the Capping Behavior of Surfactant at Ambient Conditions

Mandeep Singh Bakshi,*,†,‡,# Shweta Sachar,# Gurpreet Kaur,# Poonam Bhandari,#
Gurinder Kaur,‖ Mark C. Biesinger,§ Fred Possmayer,‡ and Nils O. Petersen*,†,⊥

*Department of Chemistry, Department of Biochemistry, and Surface Science Western, Room G1,
Western Science Centre, University of Western Ontario, 339 Windermere Rd, London, ON, Canada
N6A 5A5, Department of Physics, College of North Atlantic, Labrador City, A2V 2K7 NF, Canada,
National Institute for Nanotechnology, Edmonton, Alberta, Canada, and Department of Chemistry,
Guru Nanak Dev University, Amritsar 143005, Punjab, India*

**ABSTRACT:** A seed-mediated approach was applied to synthesize gold (Au) nanoparticles (NP) by using twin tail alkylammonium cationic surfactants such as 12-6-12 and 12-0-12 as capping agents in aqueous phase at ambient conditions. The growth of Au NP was monitored by changing the amount of seed. Spherical NP (10–50nm) and nanorods (aspect ratio = 2–3) were obtained in the presence of 12-6-12 as capping agent; their shape and size systematically deformed because of anisotropic growth with a decrease in the amount of seed. In contrast, when 12-0-12 was used as a capping agent, no anisotropic growth was observed. An effective liquid/solid interfacial adsorption of 12-0-12 prevented anisotropic growth which led to precise morphologies. This was not observed in the case of 12-6-12 because of the presence of a spacer which restricted an effective interfacial adsorption because of the steric factors. XPS and FTIR studies clearly indicated the presence of a surfactant film on the surface of Au NP, while XRD analysis demonstrated a difference in the preferential adsorption of 12-6-12 and 12-0-12 at different crystal planes of fcc geometry which resulted in a difference in their capping behaviors.

## Introduction

Morphology control is the main objective in the development of advanced nanomaterials.[1] The seed-mediated approach has become increasingly popular recently[2] in the production of ordered morphologies of Au NP in aqueous surfactant solutions. A systematic growth of Au NP requires weak reducing conditions and appropriate selection of a capping agent. Some studies[3] have successfully controlled the size distribution (typically 10–15%) in the range of 5–40 nm by manipulating the ratio of seed to metal salt. Step-by-step particle enlargement is more effective than a single-step seeding method to avoid secondary nucleation.[4] In a seed-growth method, small metal NP are prepared first and later used as seeds (nucleation centers) for a systematic growth of large sized NP. Such methods have been successfully applied for shape -controlled synthesis of Au, Ag, Ir, Pd, and Pt NP.[5] However, finding a suitable growth condition that inhibits additional nucleation generally limits the application of such methods.[6,7] The secondary nucleation mostly leads to anisotropic growth which can be controlled by a selective adsorption of surfactant ions on specific crystal planes. For instance, cetyltrimethylammonium bromide (CTAB)[2a–c] prefers to adsorb at {100} facets of fcc geometry of Au or Ag NP and hence directs the growth at {111} crystal planes to form nanorods or nanowires. Because the adsorption of a cationic surfactant like CTAB on specific crystal planes governs by electrostatic interactions, polarity of the surfactant headgroup plays an important role in an effective capping process.

Quaternary ammonium Gemini surfactants[8] are basically dimeric homologues of monomeric cationic surfactants. They are much more hydrophobic than their monomeric homologues.[9] Greater hydrophobicity in fact provides a driving force for a stronger liquid/solid interfacial adsorption and that is important for a shape controlled synthesis. Because the surfactant adsorption, for instance at {100} crystal planes of fcc geometry, is electrostatically controlled, polarity of an ionic headgroup plays an important role. It becomes a prominent factor when the surfactant is dimeric in nature like a Gemini surfactant. Although, there are few studies[10] of Au NP formation by using Gemini surfactants in the literature, little is known about the role of Gemini headgroup as far as their surface adsorption is concerned. We have undertaken a comprehensive study to quantitatively evaluate the effect of Gemini headgroup on shape-controlled synthesis by comparison of the capping ability of bis (alkyl ammonium) bromides such as 12-6-12 and 12-0-12. 12-6-12 possesses a dimeric ammonium headgroup with a hydrophobic spacer of 6 methylene groups, while 12-0-12 has no spacer and is monomeric. Because both surfactants have C12 twin hydrocarbon tails, the degree of liquid/solid interfacial adsorption would only be controlled by the nature of their head groups and that would, in turn, affect the overall crystal growth.

## Experimental Section

**Materials.** Tetrachloroauric acid (HAuCl4), sodium borohydride (NaBH4), and trisodium citrate (Na3Cit) were obtained from Aldrich. Hexamethylene-1,6-bis(dodecyldimethylammonium bromide) (12-6-12) and didodecyldimethylammonium bromide (12-0-12) were synthesized as reported in the literature[11] and used after repeated crystallization from ethanol. The molecular structures of both 12-6-12 and 12-0-12 have been shown in Scheme 1. Ultra pure water (18 MΩ cm) was used for all aqueous preparations.

**Synthesis of 12-6-12/12-0-12 Capped Au NP by Seed-Growth (S-G) Method.** The S-G method used here (Scheme I, SI, Supporting Information) is essentially similar to that reported by Murphy et al.[12] Briefly, the preparation of a seed solution includes 25 mL of HAuCl4 aqueous solution ([HAuCl4] = 0.5 mM) in a screw-capped glass bottle along with [Na3Cit] = 0.5 mM. The addition of 0.6 mL of aqueous NaBH4 ([NaBH4] = 0.1 mol dm$^{-3}$) solution led to a ruby red color to

*To whom correspondence should be addressed. E-mail: ms_bakshi@ yahoo.com (M.S.B.); Nils.Petersen@nrc-cnrc.gc.ca (N.O.P.).
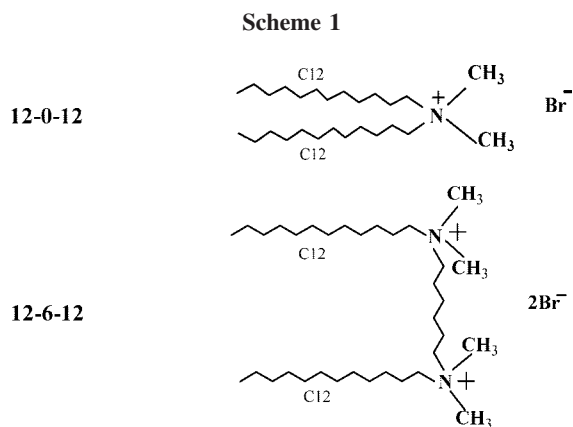† Department of Chemistry, University of Western Ontario.
‡ Department of Biochemistry, University of Western Ontario.
§ Surface Science Western, University of Western Ontario.
‖ Department of Physics, College of North Atlantic.
⊥ National Institute for Nanotechnology.
# Department of Chemistry, Guru Nanak Dev University.

**Scheme 1**

**12-0-12**

**12-6-12**

the final solution. The growth solution was prepared by taking 5 mL of [12-6-12] = 0.5 mM (critical micelle concentration, $cmc_{12\text{-}6\text{-}12}$ = 1.2 mM)[10e] and [$HAuCl_4$] = 0.5 mM in three glass tubes, that is, G1, G2, and G3. Then 0.2 mL of freshly prepared ascorbic acid (AA) aqueous solution ([AA] = 0.1 M) was added in each tube. Immediately after this, in tube G1, 0.5 mL of previously made seed solution was added, and the solution was mixed couple of times. After 1 min of time interval, 0.5 mL of solution from G1 was taken out and added into G2 and then similarly from G2 to G3. In this way, *three steps* were performed, and all G1, G2, and G3 solutions were kept in dark undisturbed to avoid photoreduction for at least two days. Similar reaction sequences with *three steps* were carried out by using 0.25 (G4–G6) and 0.125 mL (G7–G9) of seed solutions. Identical reaction series, namely, H1–H3, H4–H6, and H7–H9, by using 0.5, 0.25, and 0.125 mL of the same seed solutions, respectively, were carried out in the presence of 12-0-12 = 0.5 mM ($cmc_{12\text{-}0\text{-}12}$ = 0.2 mM)[10e] as a capping agent. In this way, three reaction sequences of G and H series of reactions were separately carried out, and Table 1 summarizes various components of all reactions along with different shapes and structures of Au NP obtained.

**Methods.** UV–visible spectra of prepared NP solutions were taken by UV spectrophotometer (Multiskan Spectrum, model no. 1500) in the wavelength range of 200–900nm to determine the absorbance caused by surface plasmon resonance (SPR). The formation of Au NP was monitored in the visible absorption range around 520nm. The shape and size of Au NP were characterized by transmission electron microscopy (TEM). Samples were prepared by mounting a drop of NP solution on a carbon-coated Cu grid and allowing it to dry in air. They were observed with the help of a Philips CM10 TEM operating at 100kV. The X-ray diffraction (XRD) patterns were characterized by using Bruker-AXS D8-GADDS with $T_{sec}$ = 480. FTIR spectra were taken by using FTIR spectrometer (Shimadzu) in the range of 4000–400 $cm^{-1}$. A few drops of a concentrated aqueous Au NP solution were placed in the center of a clean silicon wafer equal to the size of spectrophotometer window. The sample was dried by keeping it in the vacuum oven and then loaded on the spectrophotometer window. Each spectrum was measured in transmission mode with 256 scans and 4 $cm^{-1}$ resolution. The chemical composition of some samples containing Au was confirmed with the help of X-ray photoelectron spectroscopic (XPS) measurements. A portion of an aqueous NP solution was placed onto a clean silicon wafer and then it was put into the introduction chamber of the XPS instrument. The liquid was then pumped away. The XPS analyses were carried out with a Kratos Axis Ultra spectrometer using a monochromatic Al Kα source (15 mA, 14 kV). The instrument work function was calibrated to give a binding energy (BE) of 83.96 eV for the Au $4f_{7/2}$ line for metallic gold and the spectrometer dispersion was adjusted to give a BE of 932.62 eV for the Cu $2p_{3/2}$ line of metallic copper. The Kratos charge neutralizer system was used on all samples. Survey and high-resolution analyses were carried out with an analysis area of ~300 × 700 $\mu$m using pass energies of 160 and 20 eV, respectively. Special care was taken to completely remove the uncapped surfactant from each sample used for FTIR and XPS measurements.

## Results

**UV–visible Measurements.** Au NP provide a sharp absorbance in the visible region around 520nm. The shape of the resonance peak can be qualitatively related to the nature of NP. Small and uniform-sized NP with narrow size distribution give a sharp absorbance, while NP with wide size distribution or any kind of aggregation show a broad absorbance.[13] Figure 1a and b shows the UV–visible absorbance of 12-6-12 and 12-0-12 capped Au NP, respectively. Figure 1a shows the absorbance of Au NP made with 0.5 mL seed solution with a complete reaction sequence of G1−G3. For samples G1 and G2, the sharp absorbance located at 520nm is caused by the presence of small spherical NP. Another shoulder for G2 at higher wavelength (~720 nm) is the result of longitudinal SPR of rod-shaped (nanorods, NR) NP.[14] It is not possible to identify the absorbance only resulting from the transverse SPR of NR because of the presence of spherical NP. Therefore, the magnitude of the absorbance intensity at 520nm is much larger than that of the longitudinal SPR. For the G3 sample, both absorbances show a red shift of ~30 nm, indicating a relative increase in the size of both kinds of NP. On the other hand, although similar reactions for H series of samples (Figure 1b) show sharp absorbances resulting from spherical NP of H1 and H2 at 530nm, no shoulder caused by longitudinal SPR of NR is observed for H2. The absorbance of H3, like that of G3, is slightly red-shifted, and H3 also shows a prominent shoulder resulting from longitudinal SPR. A comparison between the absorbances of two series of corresponding G and H samples indicate a clear difference in the absorbance wavelength of longitudinal SPR. The absorbance for G3 is more than 100 nm red-shifted from that of H3 and might be caused by some ordered arrangement[14] (this will be explained along with TEM images in next section). Essentially, a similar comparison can be made between other sets of G (G4–G6 and G7–G9) and H (H4–H6 and H7–H9) series of samples where identical amounts of seed solutions were used (not shown).

**TEM Measurements.** All TEM images of G samples (12-6-12) have been compared with H samples (12-0-12) to drive a precise conclusion on the basis of a spacer effect of Gemini surfactants. First of all, *step 1* of three reaction sequences (i.e., G1, G4, G7 for G and H1, H4, H7 for H samples) has been compared in Figure 2. All G1, G4, and G7 samples have identical amounts of ingredients, except seed solution, which is 0.5, 0.25, and 0.125 mL, respectively. The same situation exits for H1, H4, and H7 samples. The size distribution histogram for each sample is shown in Figure S1, SI. It is to be mentioned that the size distribution histogram for each sample was manually calculated to clearly quantify the various morphologies. For G1, mostly small spherical NP (10.6 ± 3.5 nm) are obtained, which become slightly bigger (12.3 ± 2.0 nm) for G4, along with the presence of NR (aspect ratio = 1.97 ± 0.35). For G7, the size of both particles (sphere = 19.1 ± 3.6 nm; NR = 3.16 ± 0.67) further increases. In the case of corresponding H series of samples (corresponding histograms in Figure S2, SI), H1 contains mostly spherical NP (10.6 ± 3.6 nm) which slightly grow in size (12.9 ± 2.5 nm) for H4. Here, unlike the formation of NR as it happened in the case of G4, many triangular NP (12.7 ± 3.3 nm) are also obtained along with spheres and few NR (aspect ratio = 1.7 ± 0.37). In H7, the size increases for sphere, triangle, and NR (Table 1, respective histograms, Figure S2$_{H7a,b,c}$, SI), but this sample now also contains few hexagons. Thus, a relative comparison between the corresponding G and H series of samples suggests a clear shape evolution (sphere, rod, triangle, hexagon) in the NP of H series of samples with 12-0-12 as a capping agent, while only spheres and rods are obtained in G series of samples with 12-6-12 as a capping agent.

**Table 1. specifications of all samples of S-G Reaction Sequences in the Presence of 12-6-12 (G samples) and 12-0-12 (H samples) and the Shape and Size of Gold Nanoparticles of Each Sample[a]**

| sample no. | | seed (mL) | G samples | | H samples | |
|---|---|---|---|---|---|---|
| | | | NP shape and size[b] | % NP | NP shape and size[b] | % NP |
| G1 | H1 | 0.5 | S, 10.6 ± 3.5 nm | | S, 10.6 ± 3.6 nm | |
| G2 | H2 | 0.5 | S, 24.3 ± 6.2 nm; R, 2.71 ± 0.67 | S = 49, R = 51 | S, 28.7 ± 3.2 nm; T, 37.4 ± 9.9 nm; H, 23.7 ± 3.7 nm; R, 2.98 ± 0.87 | S = 43, T = 18, H = 28, R = 11 |
| G3 | H3 | 0.5 | S, 56.5 ± 12.9 nm; R, 2.29 ± 0.97 | S = 78, R = 22 | S, 45.4 ± 16.6 nm; T, 33.3 ± 8.7 nm; H, 27.2 ± 4.4 nm; R, 2.20 ± 0.44 | S = 6, T = 11, H = 32, R = 50 |
| G4 | H4 | 0.25 | S, 12.3 ± 2.0 m; R, 1.97 ± 0.35 | S = 74, R = 26 | S, 12.9 ± 2.5 nm; T, 12.7 ± 3.3 nm; R, 1.7 ± 0.37 | S = 92, T = 6, R = 2 |
| G5 | H5 | 0.25 | S, 40.3 ± 11.2 nm; R, 3.05 ± 0.57 | S = 54, R = 46 | S, 38.0 ± 4.6 nm; T, 61.1 ± 6.5 nm; H, 23.3 ± 1.4 nm; R, 3.53 ± 0.84 | S = 33, T = 10, H = 32, R = 25 |
| G6 | H6 | 0.25 | S, 154 ± 22.8 nm | | S, 85.0 ± 27.6 nm; T, 84.6 ± 26.2 nm; H, 67.6 ± 9.4 nm; R, 3.23 ± 1.34 | S = 15, T = 15, H = 38, R = 31 |
| G7 | H7 | 0.125 | S, 19.1 ± 3.6 nm; R, 3.16 ± 0.67 | S = 70, R = 30 | S, 19.3 ± 2.5 nm; T, 23.3 ± 8.9 nm; H, 20.5 ± 4.3 nm; R, 2.1 ± 0.54 | S = 91, T = 2, H = 4, R = 3 |
| G8 | H8 | 0.125 | S, 58.7 ± 26.6 nm; R, 2.45 ± 0.73 | S = 84, R = 16 | S, 66.0 ± 24.6 nm; T, 85.8 ± 19.1 nm; H, 65.0 ± 17.4 nm; R, 2.81 ± 0.59 | S = 25, T = 6, H = 14, R = 55 |
| G9 | H9 | 0.125 | S, 250 ± 49.3 nm | | S, 65.0 ± 12.9 nm; T, 47.1 ± 7.2 nm; H, 42.5 ± 8.4 nm; R, 2.69 ± 0.75 | S = 40, T = 11, H = 13, R = 23 |

[a] S → sphere, T → triangle, H → hexagonal, and R → rod. [b] The size of rod is in aspect ratio.
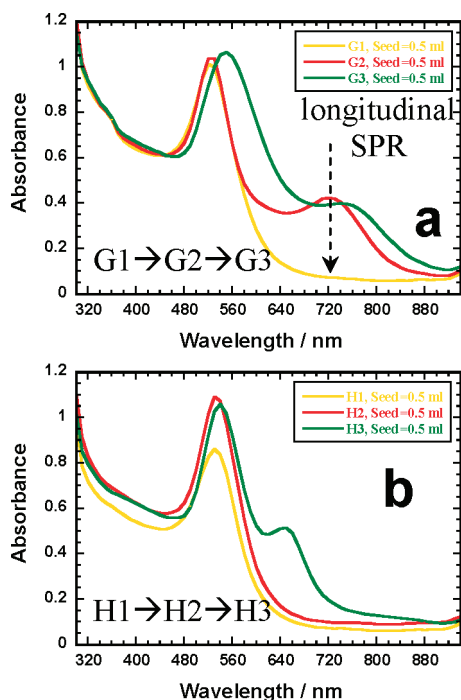


**Figure 1.** UV–visible absorption spectra showing the absorbance of (a) 12-6-12 capped Au NP with a complete reaction sequence of G1−G3 with 0.5 mL of seed solution and (b) the corresponding reactions for H1−H3 of 12-0-12.

Likewise if we compare the samples of *step 2* (Figure 3) for both series of reactions as the amount of seed solution decreases (i.e., G2 > G5 > G8 and H2 > H5 > H8), the shapes of spheres and NR are very clear in G2 but start distorting in G5 and attain significant distortion in G8. The size of spheres increases from G2 to G8 (Table 1 and Figure S3, SI). A close inspection of NP of sample G5 indicates that spheres have become polyhedral, while NR have attained rounded instead of sharp ends. The NP of sample G8 have attained highly significant polyhedral

geometries, while NR become dumbbell shapes.[15,16] In contrast, this is not so in the case of corresponding H series of samples. Here, different morphologies such as sphere, triangle, hexagon, and rod are now very prominent and clearly visible in the H2 sample. The nanorods seem to have penta-twin facets. Interestingly, the shape evolution becomes more clear and size increases (see TEM for H5 and H8) for all shapes as the amount of seed decreases in the order of H2 > H5 > H8 (Table 1 and Figure S4, SI). The percent yields of different kinds of morphologies have been listed in Table 1. The yield of spheres, triangles, and hexagons predominantly decreases from H2 to H8 while that of NR increases. It means NR grows at the expense of all other morphologies as the amount of seed decreases from 0.5 to 0.125 mL. Apart from this, no dumbbell or polyhedral geometries are observed in these samples. Thus, *step 2* gives a clear indication that the crystal growth is very much affected by a significant difference in the capping ability of 12-6-12 (G2–G8) and 12-0-12 (H2−H8).

At *step 3* (Figure 4), the shape distortion becomes very prominent especially for G6 and G9 and clearly points to anisotropic growth. Interestingly, different morphologies of Au NP in the corresponding H6 and H9 samples do not show any sign of anisotropic growth.

All results have been put in Figure 5 to systematically understand the capping behavior in terms of the crystal growth. Figure 5 shows a qualitative comparison between the size of spheres (upper frame) and rods (lower frame) of both series of samples. A similar comparison of triangles and hexagons cannot be made since such shapes are absent in G series of samples. It is interesting to note that for G series of samples, the size of sphere increases from *step 1* to *step 3* in a particular reaction sequence at a fixed amount of seed and with a decrease in the amount of seed from 0.5 to 0.125 mL. On the other hand, for H series of samples, although size of spheres increases from *step 1* to *step 2*, it decreases as the amount of seed decreases from 0.25 to 0.125 mL (see the curve fitting). The overall size of spheres at each step is predominantly larger for G series of samples rather than H series. For NR (lower frame), the aspect
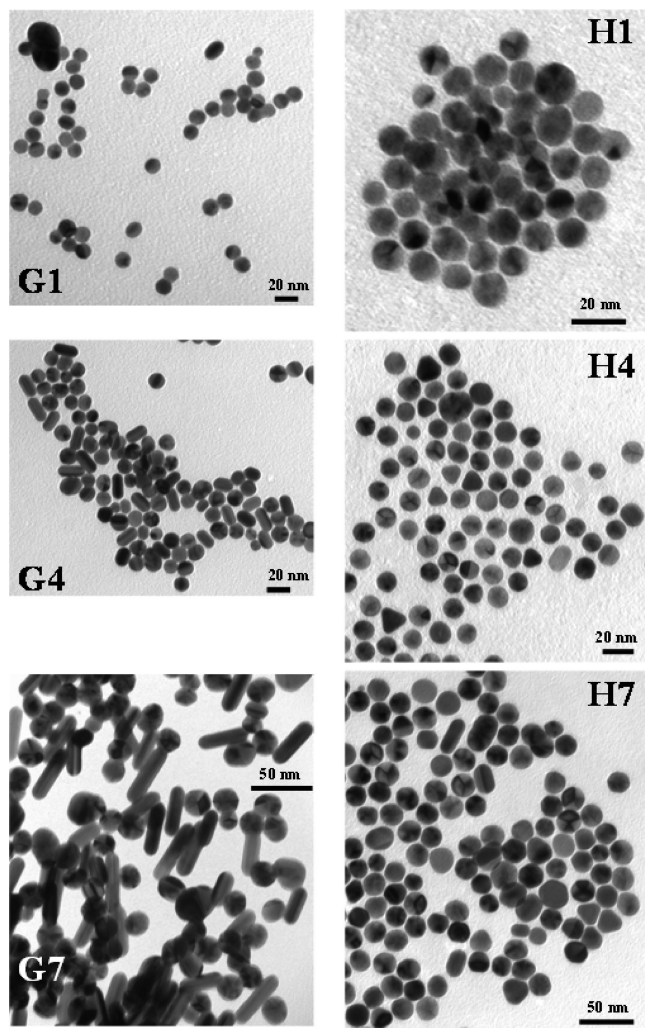
**Figure 2.** Comparison between the TEM micrographs of step 1 of G series (G1, G4, and G7) (left panels) and H series (H1, H4, and H7) (right panels) of samples (see detail in text).

ratio increases from step 1 to step 2 and then decreases to step 3 in each reaction sequence at fixed amount of seed essentially for both G and H series of samples, but the overall aspect ratio for H series of samples is predominantly higher than that of G series of samples. This is mainly caused by the dumbbell-shaped NR formation in the G series of samples.

**FT-IR and XPS Measurements.** To quantify the surface adsorption of 12-6-12/12-0-12 on Au NP surface, FTIR spectral studies of some G (G2, G5, and G8) and H (H2, H5, and H8) series of samples have been carried out. Figure S5 shows representative examples of FTIR spectra of pure 12-6-12/12-0-12 and that of respective samples G2 and H2. Similar spectra were observed for other samples (not shown). The peaks at 975, 948, and 898 $cm^{-1}$ in the case of pure 12-6-12 can be assigned to the $C-N^+$ stretching modes. These peaks shift to 1107, 967, and 883 $cm^{-1}$ for G2; 1107, 966, and 891 $cm^{-1}$ for G5; and 1109, 962, and 891 $cm^{-1}$ for G8; respectively, suggesting 12-6-12 head groups are directed at the Au NP surface. Similar, behavior is demonstrated by $C-N^+$ stretching modes of 12-0-12 for H2, H5, and H8. Apart from this, the peak at 721 $cm^{-1}$ in pure 12-6-12/12-0-12 arises from the rocking mode of the methylene $(-CH_2-)_n$ chain, which shifts to higher frequencies for both G and H series of samples indicating the presence of much ordered arrangement of surfactant hydrophobic tails on the Au surface in the form of a surfactant capping film.
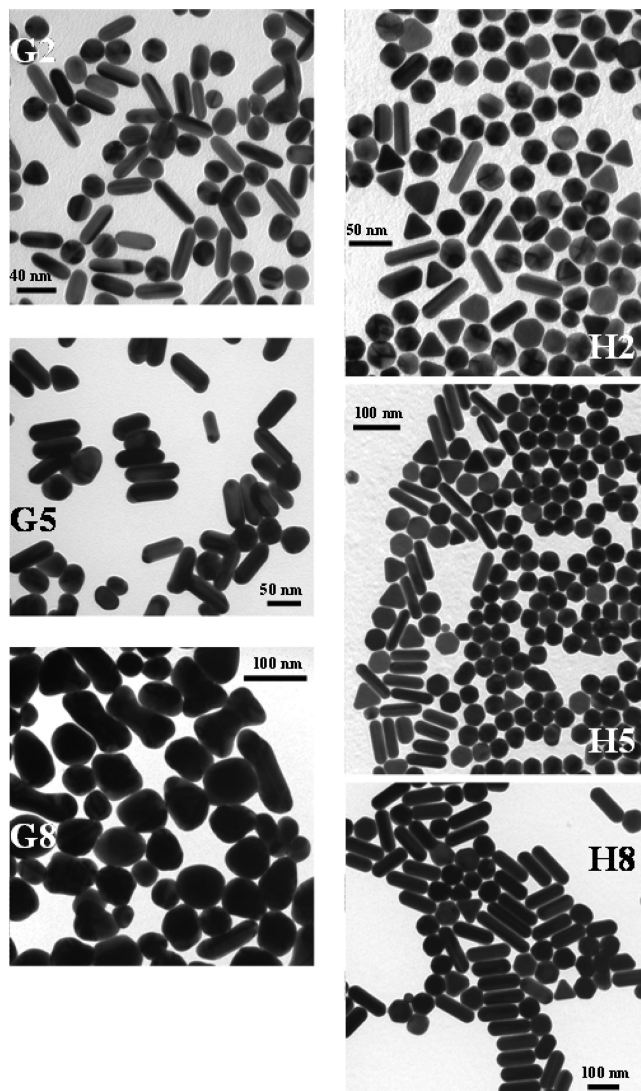


**Figure 3.** Comparison between the TEM micrographs of step 2 of G series (G2, G5, and G8) (left panels) and H series (H2, H5, and H8) (right panels) of samples (see detail in text). Note the dumbbell shaped NR in G8.

Head groups of surfactant molecules directed at Au surface are further evident from N 1s emission peak of XPS spectrum (low-resolution XPS spectra of G4 and H5 as representative examples have been shown in Figures S6 and S7, SI, and the corresponding binding energies and area occupied by various species of all samples have been listed in Table 2). Panel a, Figure 6 shows the N 1s peak of G4 which appears in the form of a doublet with binding energies at 402.0 and 398.83 eV and possessing 66.5% and 33.5% contributions, respectively. Similar doublets with corresponding contributions have been observed for other samples (Table 2). The peak around 399 eV can be attributed to free or bound amine[17] because its binding energy falls in the range of 398–400 eV, while the peak at a relatively higher energy, ~402 eV, indicates the electrostatic interactions between the charged $-N(CH_3)_3^+$ species and Au NP surface.[18] Panel b shows strong emission caused by C 1s of G4, which has been deconvoluted into number of components. Several species of C 1s from different functional groups constitute this strong emission. The percentage area occupied by each species indicates that maximum emission (~78.8%) comes from $C-C$ and $C-H$ functional groups at 284.15 eV, which constitute the hydrophobic tails of 12-6-12. Other weak emissions at 287.82
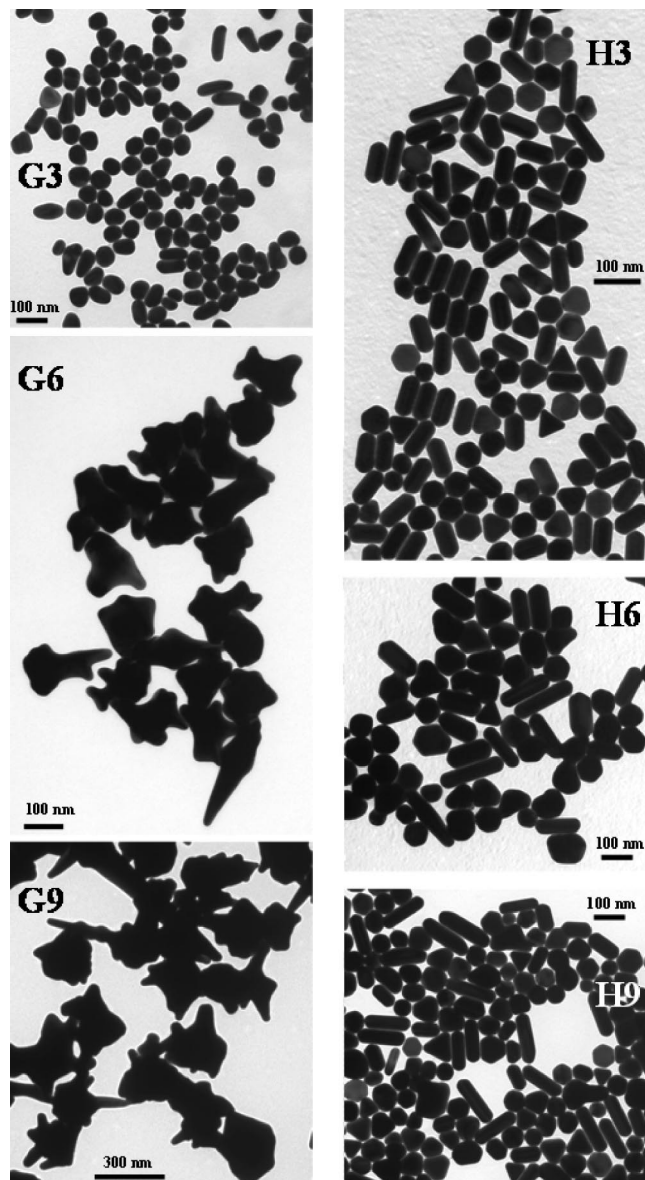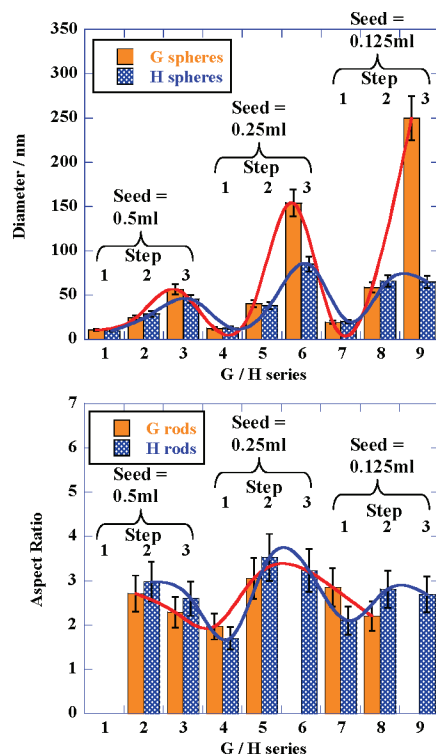
**Figure 4.** Comparison between the TEM micrographs of step 3 of G series (G3, G6, and G9) (left panels) and H series (H3, H6, and H9) (right panels) of samples (see detail in text). Note the anisotropic growth in G6 and G9.



**Figure 5.** Upper frame shows the size distribution histogram of all G and H series of samples of three reaction sequences at different seed amounts for spherical NP only. Lines are the fitting of data in order to compare the size among various Au NP from one sample to another. Lower frame shows a similar plot for nanorods. Samples G1, H1, G6, and G9, do not show clear nanorod formation; therefore their data is not listed. Error bars refer to the standard deviations in each case (see detail in text).

and 286.01 eV are caused by C=O and C−OH, respectively, of adsorbed citrate ions. The relative amount of N 1s (N/Au) increases from G4 to G6 which is almost in line with the increase in the amount of C 1s (C/Au) (Table 2). It suggests that the Au NP of both series of samples have 12-6-12/12-0-12 surfactant coating around them.

## Discussion

A collective analysis of all results from different studies point to a fundamental difference between the capping behavior of 12-6-12 and 12-0-12. This difference only arises from the presence of the spacer and the dimeric nature of 12-6-12 and from it having a completely different mode of surface adsorption than 12-0-12. We know that the stability of individual planes of fcc geometry decreases in the order of {111}>{100}>{110}[15] because of an increasing interatomic distance or decreasing surface atomic density. This provides {110} planes with highest surface energy to interact favorably with surfactant

molecules. But during the crystal growth, low-energy {111} planes are more favored because of greater stability. XRD patterns of G4, G5, and G6 (Figure 7a) and that of H4, H5, and H6 (Figure S8, SI) show a predominant crystal growth at {111} facets along with a less-prominent growth at other planes of fcc geometry. Plots of (111)/(200) and (111)/(220) intensity ratios with respect to order of crystal growth from step 1 to step 3 within a same reaction (Figure 7b and c) supports this argument. For the G series of samples, both ratios increase though the increase is substantial in the former case which clearly points to a predominant growth at {111} planes. Actually, this is the reason why the size of spherical particles increases for G series of samples (Figure 5) in comparison to that of H series of samples. However, a decrease in the aspect ratio of G series of samples is the result of them acquiring dumbbell shapes. In contrast, a decrease in the size of H series of samples is simultaneously supplemented by the triangular and hexagonal NP formation, and there is no sign of dumbbell NR formation as well. These samples indicate a predominant growth at {100} or {110} facets in comparison to {111} (Figure 7b and c). Adsorption of Au (III) and Au (I) intermediates at staking faulty or twinning plane helps in the development of facets that might favor different geometries.[12,19,20] Thus a difference in the surface adsorption among 12-6-12 and 12-0-12 holds a key for a specified growth.

The preference for {100} surface is perfectly working at step 1 for all G series of reactions (i.e., fine spheres and NR are obtained for G4), but their shapes start distorting at step 2 (G5) and step 3 (G6), and the effect is very much prominent with substantial anisotropic growth for G6. It demonstrates that 12-

**Table 2. Binding Energies (eV; I) and Area (%; II) of Some Species Constituting the Surface Composition of Au NP for G and H Series of Samples[a]**
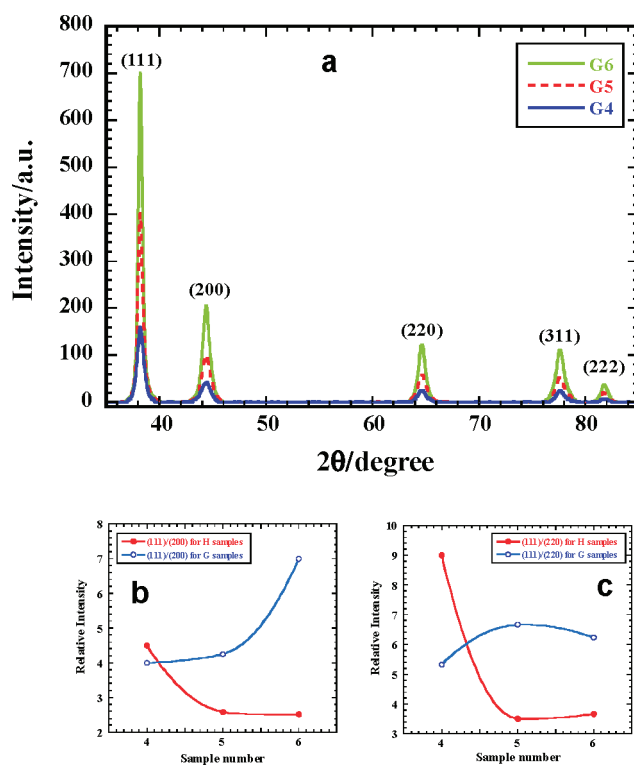
| sample | Au 4f$_{5/2}$ | | Au 4f$_{7/2}$ | | O 1s | | | | O/Au | C 1s (C–C, C–H) | | C/Au | N 1s | | | | N/Au |
|---|---|---|---|---|---|---|---|---|---|---|---|---|---|---|---|---|---|
| | I | II | I | II | I | II | I | II | | I | II | | I | II | I | II | |
| G4 | 87.72 | 15.4 | 84.05 | 20.6 | 532.03 | 42.3 | 530.35 | 57.7 | 8.5 | 284.15 | 78.8 | 43 | 402.00 | 66.5 | 398.83 | 33.5 | 1.5 |
| | 87.42 | 27.4 | 83.75 | 36.6 | | | | | | | | | | | | | |
| G5 | 87.81 | 42.8 | 84.14 | 57.2 | 532.16 | 61.5 | 530.53 | 38.5 | 7.2 | 284.66 | 69.6 | 41 | 402.12 | 70.0 | 399.08 | 30.0 | 1.8 |
| G6 | 87.71 | 17.2 | 84.04 | 23.0 | | | | | 3.2 | 284.30 | 81.2 | 98 | 401.65 | 62.6 | 398.50 | 37.6 | 4.9 |
| | 87.00 | 25.6 | 83.33 | 34.2 | | | 530.95 | | | | | | | | | | |
| H4 | 87.79 | 42.8 | 84.12 | 57.2 | 532.45 | 70.3 | 530.27 | 29.7 | 17 | 284.77 | 63.4 | 43 | - | | - | | 0.23 |
| H5 | 88.02 | 42.8 | 84.35 | 57.2 | 532.09 | 57.4 | 530.56 | 42.6 | 35 | 284.54 | 68.9 | 69 | 402.09 | 38.1 | 399.06 | 61.9 | 2.1 |
| H6 | 87.82 | 42.8 | 84.15 | 57.2 | 532.62 | 85.0 | 530.68 | 15.0 | 2.7 | 285.19 | 90.5 | 8 | 402.54 | 57.7 | 399.46 | 42.3 | 0.18 |

[a] O/Au, C/Au, and N/Au represent the atomic percent ratio.
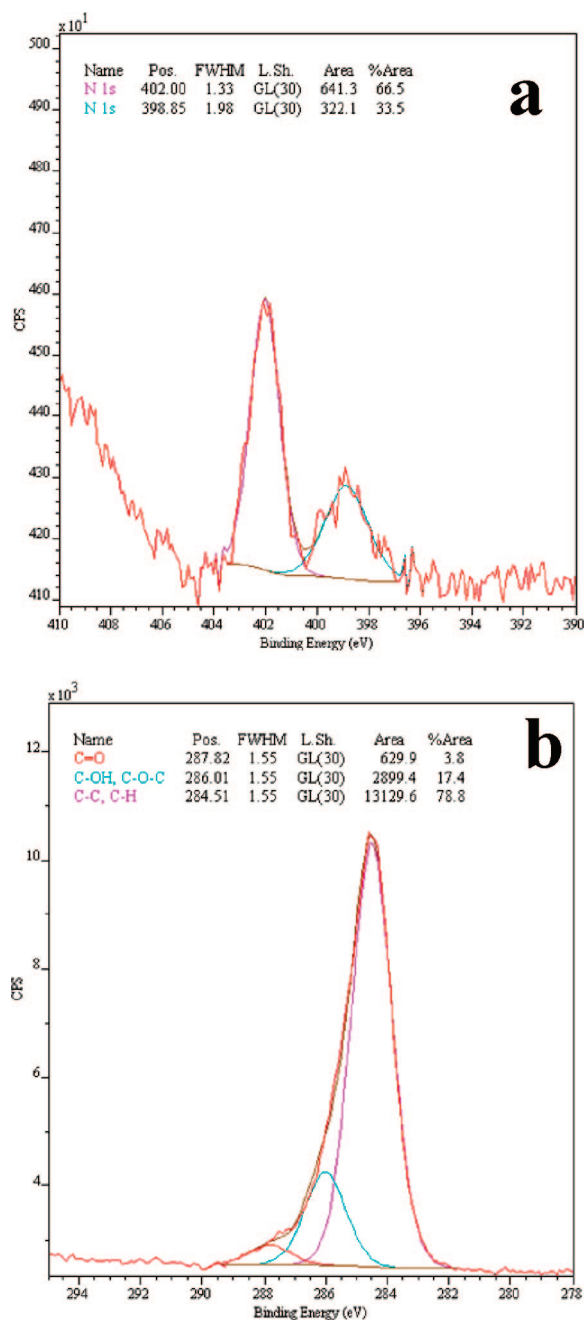


**Figure 6.** High resolution XPS spectra for N 1s (panel a) and C 1s (panel b) (see detail in text, and Table 2).



**Figure 7.** (a) XRD patterns of Au NP for G4, G5, and G6. Panels b and c show a variation in the intensity ratios of (111)/(200) and (111)/(220), respectively, of G (G4, G5, and G6) and H (H4, H5, and H6) series of samples.

formation of high aspect ratio.[2a] A spacer group of 6 methylenes embedded in the headgroup of 12-6-12 creates steric hindrances[21] during a perfect monolayer formation and might be responsible for improper monolayer formation during a crystal growth along <111> directions. Thus, it may cause excessive uncontrolled nucleation along <111> directions leading to the formation of dumbbell morphologies at step 2 (G5/G8) and that subsequently acquire anisotropic growth at step 3 (G6/G9).

## Conclusions

It is concluded that the nature of capping surfactant significantly influences the morphology of Au NP. Only spheres and NR are produced in the presence of 12-6-12, while fine morphologies of different shapes are obtained in the presence of 12-0-12. 12-6-12 though controls the shape and structure at step 1 of each reaction sequence, it cannot control the crystal growth in the subsequent steps of the S-G reaction resulting in anisotropic morphologies. This has been attributed to the imperfect monolayer formation at {100} facets of fcc geometry

6-12 cannot fully protect the {100} surface planes with proper monolayer formation during crystal growth along <111> planes of fcc geometry. Otherwise, it would have led to fine NR

because of steric hindrances created by a spacer of 6-methylenes of 12-6-12. On the contrary, this is not the case with 12-0-12 because of the absence of spacer and hence, it produces fine morphologies of different shapes without any sign of anisotropic growth.

**Supporting Information Available:** A flow diagram of seed-growth method, histograms for various TEM figures, FTIR spectra, XPS low resolution spectra, and XRD patterns. This material is available free of charge via the Internet at http://pubs.acs.org.

## References

(1) (a) Akagi, T.; Kawamura, M.; Ueno, M.; Hiraishi, K.; Adachi, M.; Serizawa, T.; Akashi, M.; Baba, M. *J. Med. Virol* **2003**, *69*, 163. (b) Rihova, B. *Adv. Drug Delivery Rev.* **2002**, *54*, 653. (c) Hayward, R. C.; Saville, D. A.; Aksay, I. A. *Nature (London)* **2000**, *404*, 56. (d) Okubo, T. *Prog. Polym. Sci.* **1993**, *18*, 481.

(2) (a) Murphy, C. J.; San, T. K.; Gole, A. M.; Orendorff, C. J.; Gao, J. X.; Gou, L.; Hunyadi, S. E.; Li, T. *J. Phys. Chem. B* **2005**, *109*, 13857. (b) Johnson, C. J.; Dujardin, E.; Davis, S. A.; Murphy, C. J.; Mann, S. *J. Mater. Chem.* **2002**, *12*, 1765. (c) Murphy, C. J.; Gole, A. M.; Hunyadi, S. E.; Orendorff, C. J. *Inorg. Chem.* **2006**, *45*, 7544. (d) Nikoobakht, B.; El-Sayed, M. A. *Langmuir* **2001**, *17*, 6368. (e) Swami, A.; Kumar, A.; Sastry, M. *Langmuir* **2003**, *19*, 1168. (f) Teranishi, T.; Hosoe, M.; Tanaka, T.; Miyake, M. *J. Phys. Chem. B* **1999**, *103*, 3818. (g) Bakshi, M. S.; Kaura, A.; Kaur, G.; Torigoe, K.; Esumi, K. *J. Nanosci. Nanotechnol.* **2006**, *6*, 644. (h) Bakshi, M. S.; Kaura, A.; Bhandari, P.; Kaur, G.; Torigoe, K.; Esumi, K. *J. Nanosci. Nanotechnol.* **2006**, *6*, 1405. (i) Kou, X.; Zhang, S.; Tsung, C. K.; Yeung, M. H.; Shi, Q.; Stucky, G. D.; Sun, L.; Wang, J.; Yan, C. *J. Phys. Chem.* **2006**, *110*, 16377. (j) Liu, M.; Guyot-Sionnest, P. *J. Phys. Chem.* **2005**, *109*, 22192.

(3) (a) Jana, N. R.; Gearheart, L.; Murphy, C. J. *Chem. Mater.* **2001**, *13*, 2313. (b) Sau, T. K.; Pal, A.; Jana, N. R.; Wang, Z. L.; Pal, T. *J. Nanopart. Res.* **2001**, *3*, 257. (c) Meltzer, S.; Resch, R.; Koel, B. E.; Thompson, M. E.; Madhukar, A.; Requicha, A. A. G.; Will, P. *Langmuir* **2001**, *17*, 1713.

(4) Carrot, G.; Valmalette, J. C.; Plummer, C. J. G.; Scholz, S. M.; Dutta, J.; Hofmann, H.; Hilborn, J. G. *Colloid Polym. Sci.* **1998**, *276*, 853.

(5) (a) Schneider, S.; Halbig, P.; Grau, H.; Nickel, U. *Photochem. Photobiol.* **1994**, *60*, 605. (b) Watzky, M. A.; Finke, R. G. *Chem. Mater.* **1997**, *9*, 3083. (c) Brown, K. R.; Natan, M. J. *Langmuir* **1998**, *14*, 726. (d) Brown, K. R.; Walter, D. G.; Natan, M. J. *Chem. Mater.* **2000**, *12*, 306. (e) Henglein, A.; Giersig, M. *J. Phys. Chem. B* **1999**, *103*, 9533. (f) Henglein, A. *Langmuir* **1999**, *15*, 6738.

(6) (a) Overbeek, J. Th. G. *Adv. Colloid Interface Sci.* **1982**, *15*, 251. (b) Wiesner, J.; Wokaun, A. *Chem. Phys. Lett.* **1989**, *157*, 569.

(7) Jana, N. R. *Small* **2005**, *1*, 875.

(8) (a) Menger, F. M.; Littau, C. A. *J. Am. Chem. Soc.* **1991**, *113*, 1451. (b) Bai, G.; Wang, J.; Yan, H.; Li, Z.; Thomas, R. K. *J. Phys. Chem. B.* **2001**, *105*, 3105. (c) Zana, R. *Adv. Colloid Interface Sci.* **2005**, *97*, 205.

(9) (a) Bakshi, M. S.; Singh, J.; Kaur, G. *J. Colloid Interface Sci.* **2004**, *285*, 403. (b) Bakshi, M. S.; Sachar, S. *Colloid Polym. Sci.* **2005**, *224*, 671. (c) Bakshi, M. S.; Singh, J.; Kaur, G. *J. Photochem. Photobiol.* **2005**, *173*, 202. (d) Bakshi, M. S.; Kaur, G. *J. Colloid Interface Sci.* **2005**, *289*, 551.

(10) (a) Esumi, K.; Hara, J.; Aihara, N.; Usui, K.; Torigoe, K. *J. Colloid Interface Sci.* **1998**, *208*, 578. (b) Zhang, L.; Sun, X.; Song, Y.; Jiang, X.; Dang, S.; Wang, E. *Langmuir* **2006**, *22*, 2838. (c) Bakshi, M. S.; Possmayer, F.; Petersen, N. O. *Chem. Mater.* **2007**, *19*, 1257. (d) Bakshi, M. S.; Sharma, P.; Banipal, T. S. *Mater. Lett.* **2008**, . in press. (e) Bakshi, M. S.; Sharma, P.; Banipal, T. S.; Kaur, G.; Torigoe, K.; Petersen, N. O.; Possmayer, F. *J Nanosci. Nanotechnol.* **2007**, *7*, 916.

(11) (a) Zana, R.; Benrraou, M.; Rueff, R. *Langmuir* **1991**, *7*, 1072. (b) Wettig, S. D.; Verall, R. E. *J. Colloid Interface Sci.* **2001**, *244*, 377.

(12) Murphy, C. J.; San, T. K.; Gole, A. M.; Orendorff, C. J.; Gao, J. X.; Gou, L.; Hunyadi, S. E.; Li, T. *J. Phys. Chem. B* **2005**, *109*, 13857.

(13) (a) Liz-Marzan, L. M. *Langmuir* **2006**, *22*, 32. (b) Schultz, D. A. *Curr. Opin. Biotechnol.* **2003**, *14*, 13. (c) Sun, Y.; Xia, Y. *Analyst* **2003**, *128*, 686. (d) Schofield, C. L.; Haines, A. H.; Field, R. A.; Russell, D. A. *Langmuir* **2006**, *22*, 6707. (e) El-Sayed, M. A. *Acc. Chem. Res.* **2001**, *34*, 257. (f) Eustis, S.; El-Sayed, M. A. *Chem. Soc. Rev.* **2006**, *35*, 209.

(14) Jain, P. K.; Eustis, S.; El-Sayed, M. A. *J. Phys. Chem. B* **2006**, *110*, 18243.

(15) (a) Xiang, Y.; Wu, X.; Liu, D.; Jiang, X.; Chu, W.; Li, Z.; Ma, Y.; Zhou, W.; Xie, S. *Nano Lett.* **2006**, *6*, 2290. (b) Yu, Y. Y.; Chang, S. S.; Lee, C. L.; Wang, C. R. *J. Phys. Chem. B* **1997**, *101*, 6661. (c) Z, S.-H.; Jiang, Z.-Y.; Xie, Z.-X.; Xu, X.; Huang, R.-B.; Zheng, L.-S. *J. Phys. Chem. B* **2005**, *109*, 9416.

(16) (a) Wang, Z. L.; Mohamed, M.; Link, S.; El-Sayed, M. A. *Surf. Sci.* **1999**, *440*, L809. (b) Wang, Z. L.; Gao, R. P.; Nikoobakht, B.; El-Sayed, M. A. *J. Phys. Chem. B* **2000**, *104*, 5417.

(17) Sharma, J.; Mahima, S.; Kakade, B. A.; Pasricha, R.; Mandale, A. B.; Vijayamohanan, K. *J. Phys. Chem. B* **2004**, *108*, 13280.

(18) Sharma, J.; Chaki, N. K.; Mandale, A. B.; Pasricha, R.; Vijayamohanan, K. *J. Colloid Interface Sci.* **2004**, *272*, 145.

(19) Ni, C.; Hassan, P. A.; Kaler, E. W. *Langmuir* **2005**, *21*, 3334.

(20) Perez-Juste, J.; Liz-Marzan, L. M.; Carnie, S.; Chan, D. Y. C.; Mulvaney, P. *Adv. Funct. Mater.* **2004**, *14*, 571.

(21) (a) Bakshi, M. S.; Kaur, G.; Yoshimura, T.; Esumi, K. *Colloids Surf., A* **2006**, *281*, 163. (b) Bakshi, M. S.; Singh, K.; Kaur, G.; Yoshimura, T.; Esumi, K. *Colloids Surf.* **2006**, *278*, 129.